DEVELOPING AN EXPERIMENT CAMPAIGN TO CHARACTERIZE FIELD SITES ON THE ISLAND OF HAWAIʻI AS A LUNAR SURFACE ANALOGUE FOR ICE-PROSPECTING ROVER TESTS

A FINAL REPORT SUBMITTED TO THE DEPARTMENT OF EARTH SCIENCES, UNIVERSITY OF HAWAIʻI AT MĀNOA, IN PARTIAL FULFILLMENT OF THE REQUIREMENTS FOR THE DEGREE OF

MASTER OF SCIENCE

IN

EARTH AND PLANETARY SCIENCES

DECEMBER 2023

BY

KRYSTAL D. ARROYO-FLORES

COMMITTEE:
FRANCES ZHU, CHAIRPERSON
SHUAI LI
PAUL G. LUCEY

Abstract

The detection of water ice in the lunar South Pole regions was done using reflectance data taken via remote sensing instruments in orbit. An autonomous ice-prospecting rover on the surface would be able to explore and directly measure the terrain, determining the precise location of any water ice and creating a map of its distribution. The development of such a rover would greatly benefit from a nearby field site that is both geologically analogous to the lunar surface and capable of forming detectable water ice, as such a site would provide an accessible way to conduct performance field tests with higher fidelity than is available with simulated and laboratory environments alone. For this project, I developed an experiment campaign to gather spectral reflectance data of a prospective field site on the island of Hawai‘i and analyze it to determine if the site is sufficiently geologically similar to lunar reference data to serve as a surface analogue for the rover. I constructed a sensor suite with a field spectrometer and used it to gather reflectance data where water ice might be present at the prospective analogue site on Mauna Kea. I then analyzed the data for similarity against publicly available reference data to determine the validity of the site as an analogue. While I was not able to confirm the presence of water ice, the analysis shows high levels of similarity with anorthositic simulants and Apollo returned samples, indicating that the site is a valid geologic analogue for the lunar surface.

Table of Contents

List of Figures

List of Tables

1. INTRODUCTION

A significant focus in current lunar research is the search for water, with surface exposed water ice having been detected in the lunar South Pole regions (Li et al., 2018). While past observations have relied on data from remote sensing missions, a rover located on the lunar surface would be able to explore and measure the terrain directly and thus provide more robust data. The development of an autonomous lunar rover with the capability to search for water ice and map its distribution must include extensive operational testing, and although much of this testing can be conducted using simulated and laboratory environments, higher-fidelity performance tests of the rover hardware and software will need to be conducted in an outdoor field site (Flynn et al., 2021). For the most accurate testing as to how the rover will respond in-situ, the chosen field site should qualify as a geologic analogue for the lunar surface, as well as experience scattered distribution of water ice. As the team currently developing an ice-prospecting rover at the University of Hawai‘i at Mānoa’s Hawai‘i Institute of Geophysics and Planetology (HIGP) is located in the Hawaiian Islands, a qualifying field site in Hawai‘i would be much more convenient for testing than existing analogues located elsewhere; for example, one site that has already been used to conduct lunar spectral research is located in Holuhraun, Iceland, which would be a logistically complex and expensive undertaking for a small research team (Gwizd et al., 2023). Fittingly, sites in Hawai‘i have been used as lunar and Martian analogues in the past due to their volcanic terrain, including locations on the Big Island that were used for NASA analogue field testing operations (Sanders et al., 2011; Ten Kate et al., 2013; Yingst et al., 2015). For this project, I developed an experiment campaign to validate one of these sites as a lunar surface analogue that can be used to test the ice-prospecting rover’s exploration strategy. The campaign consists of a data-gathering method and subsequent analysis,

with the former based on the characterization of possible water ice that was previously conducted in the lunar polar regions with remote sensing (Li et al., 2018), but utilizing direct reflectance measurements taken with a field spectrometer instead. The selection of the prospective field sites was based on previous terrain characterization studies conducted by the Pacific International Space Center for Exploration Systems (PISCES) with Energy Dispersive X-Ray Fluorescence (EDXRF) (Romo et al., 2021).

2. METHODS

2.1. Sensor Suite Development

The rover's search for water ice will utilize a field spectrometer as its primary sensor: the FieldSpec4 Standard-Res from Analytical Spectral Devices (ASD). This instrument is a visible and near-infrared (VNIR) spectrometer that is meant for use both in a laboratory environment and outdoors, with a spectral range from 350-2500 nm and spectral resolution of 5 nm (Figure 1).

Figure 1: Field VNIR Spectrometer in Laboratory Setting.

To validate the field site specifically for the rover operations, I designed a sensor suite around the same spectrometer to gather the data from the field. To supplement the reflectance data from the spectrometer, I incorporated two additional sensors into the sensor suite: a GT-U7 Global Positioning System (GPS) + Patch Antenna and a GY-521 MPU-6050 Inertial Measurement

Unit, or accelerometer (IMU). Together these sensors provide continuous position, rotation, acceleration, and temperature measurements throughout the entirety of data acquisition. Power and data for both sensors are relayed between them and the operational computer via an Arduino UNO Rev3 Microcontroller Board (Figure 2).

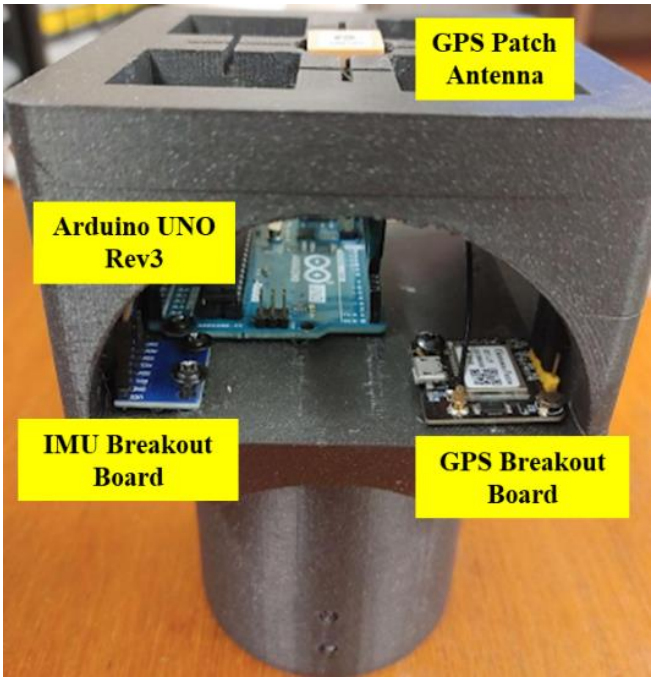

Figure 2: 3D-Printed Sensor Box Housing the IMU, GPS, and Arduino.

Designing the fully integrated sensor suite required further incorporation of spectrometer accessories, as well as consideration for how to increase measurement consistency and ease of operability while out in the field. While the sensors will ultimately be integrated into the rover body for either remote-controlled or autonomous data collection in the performance tests, for the field testing covered by this report, the suite was designed to be worn, carried, and manually operated by a human data collector. This configuration makes use of the field backpack provided by ASD along with the spectrometer, which is similar in structure to a hiking backpack and has designated features that securely house the instrument body, a rechargeable field battery, and a

spare battery, and can also suspend a sling board in front of the operator to hold the laptop while taking measurements.

To obtain the most accurate measurements possible, the fiber optic spectrometer cable must be held at a consistent angle to and distance from each target while sampling, and must also be regularly pointed at a White Reference panel to re-calibrate the instrument for any changes in environmental light (*FieldSpec 4 User Manual*, 2016). To minimize the fatigue and human error caused by manually holding the cable above each target, I designed a "Sensor Staff" to be carried by the operator in addition to the field backpack. This staff holds all of the sensor apertures at consistent positions and angles relative to both each other and the target point, and also acts as a hiking aid to the operator. The staff is constructed from a PVC pipe approximately 4 feet in length and 1.25 inches in diameter, specifications which were chosen to provide a comfortable height and grip for the operator. A 3D-printed block-shaped housing sits on the top of the pipe with a press fit (see Figure 2 and Figure 3). This housing maintains a radially symmetrical silhouette while protecting the Arduino, IMU, and GPS printed circuit boards from exposure to the environment. The GPS patch antenna is embedded within the top face of the housing in the center to achieve maximum line of sight with the nearest GPS satellites and therefore reduce the time needed to calculate a valid location. The power and data cable for the sensors connects to the Arduino directly on the -Y face of the sensor box on one end and to the laptop computer on the other.

On the lower end of the staff is a mount which holds the fiber optic cable in the ASD pistol grip accessory at a constant 0-degree angle to the staff (90 degrees to the ground surface). The spectrometer fiber optic cable in bare fiber configuration has a 25-degree field of view (FOV)

and therefore an approximate 1:2 ratio of the target diameter to the distance from the sample (Figure 4). Additionally, for proper white reference calibration, the target diameter must be no

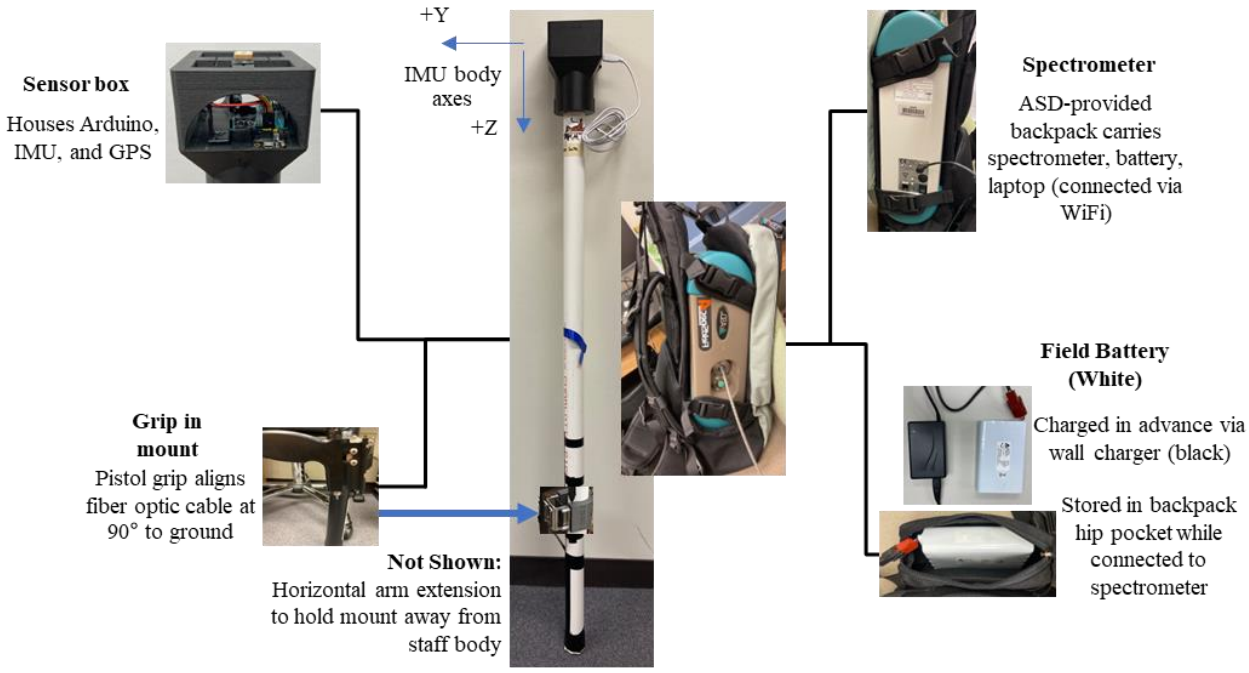

Figure 3: Sensor Suite Diagram Illustrating Positions of Components Either on the Sensor Staff or Within the Spectrometer Backpack

greater than the diameter of the white reference panel used. The Spectralon panel acquired for the rover is a square 5 inches in diameter, so this constraint resulted in a mount height of approximately 12 inches from the bottom of the staff. To avoid interference with the target diameter, the mount sits at the end of a horizontal arm, positioning the fiber-optic cable aperture approximately 7 cm away from the staff body. The arm attaches to the main staff with an easily adjustable clamp, allowing the mount height to be changed if desired, and the entire arm to be removed for storage or transportation. A second staff constructed from a slightly-smaller-in-diameter PVC pipe holds the white reference panel at both a constant vertical distance in between the fiber optic cable and the target surface, and also at a constant 90-degree angle (perpendicular) to the cable aperture, providing stability during calibration (Figure 5).

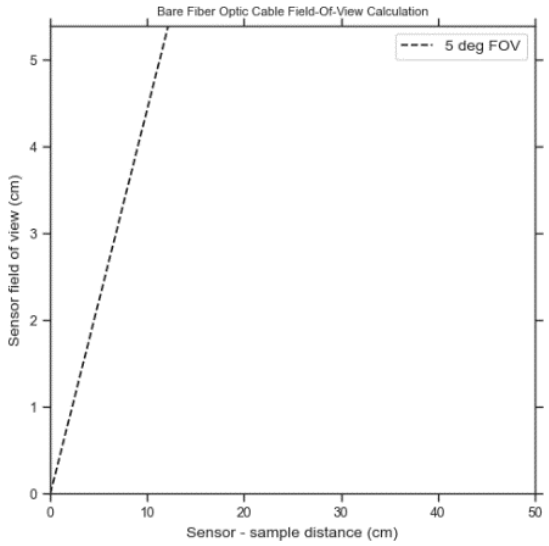

Figure 4: ASD FieldSpec4 Field of View Diagram

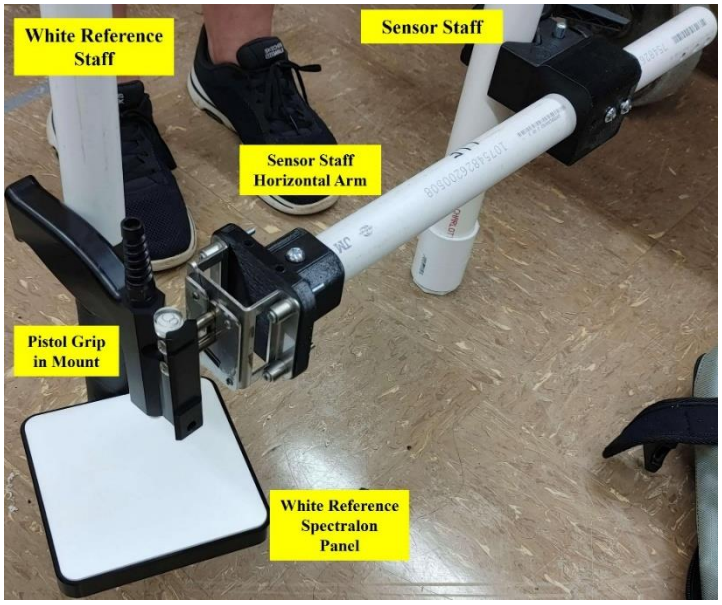

Figure 5: Sensor Staff and White Reference Staff Configuration

As the spectrometer receives power from the field battery held in the backpack's hip pocket and transmits data to the computer via a dedicated wireless connection, the sensor cable and fiber optic cable are the only two physical connections between the backpack and the main staff (an optional trigger button cable can be connected to the spectrometer accessory port and held

anywhere that is comfortable for the operator to reach, but it is not necessary for operation). The fiber optic cable is the shorter and more fragile of the two required connections, and thus is the limiting factor for how far the operator can safely stand from the target measurement (see Figure 6). The white reference staff is completely separate and so can be handled by a second team member with no limitations on distance.

Figure 6: Sensor Suite Worn by Human Operator

Throughout the development of the Sensor Suite design, I conducted various brief functional tests on the University of Hawai‘i at Mānoa campus. These tests provided feedback on the suite’s performance and operability, as well as verification of and familiarity with the requirements and procedures necessary for successful data collection. Changes that were made to the sensor suite design as a result of the campus tests include:

- Integration of and subsequent separation from a bevameter (terramechanic sensor).

- Iterations on the 3D-printed Sensor Box and pistol grip mount designs, including the addition of the horizontal arm.
- Addition of a PVC end cover to the Sensor Staff base.
- Adjustments to the mount height and distance away from the staff body.
- Creation of the separate White Reference Staff.

2.2. Field Site Selection and Access

The candidate field sites for the ice-prospecting rover's future field tests were chosen beforehand from the results of research studies conducted by the Pacific International Space Center for Exploration Systems (PISCES), which sampled and characterized the composition of terrain samples from multiple sites in Hawai‘i to determine which of them contain the most chemically similar basalt to lunar samples. The field sites also needed to be capable of reaching temperatures low enough for water ice to form on the ground, a condition which can only occur in Hawai‘i at sufficiently high elevations. Two of the PISCES sites met this additional requirement due to their locations on volcanic slopes: Pu‘uhaiwahine on Mauna Kea (19°45'33"N, 155°27′22″W) and HI-SEAS on Mauna Loa (19°36’11"N, 155°29′15″W), which are both sites on the Big Island that have been used as planetary analogues in the past (Edison et al., 2021; Romo et al., 2021). Unfortunately, access to the HI-SEAS site was endangered in the fall of 2022 following the eruption of Mauna Loa (*The 2022 Eruption of Mauna Loa*, 2023). As a result, this project includes characterization of the Pu‘uhaiwahine site alone.

The Pu‘uhaiwahine valley is located west of the Mauna Kea Visitor Information Station (VIS) and has elevations of approximately 9200 ft (the true summit of Mauna Kea sits at an elevation of 13803 ft) (Figure 7). The area falls within the Mauna Kea Forest Reserve and is

therefore under the jurisdiction of the Hawai‘i Department of Natural Land and Resources (DLNR) Division of Forestry and Wildlife (DOFW). Anyone seeking to conduct scientific research within the reserve must request and obtain a research permit from DOFW in advance. The permit for this project was granted in March 2023, allowing the data-gathering trip to occur April 7-9, 2023.

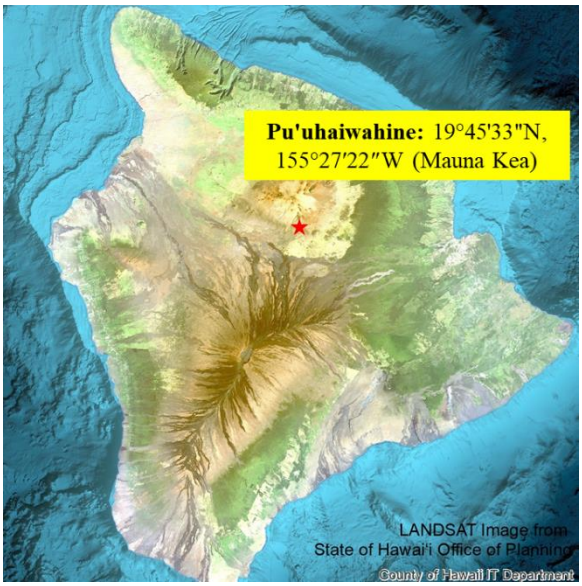

Figure 7: Analogue Field Site Location

2.3. Data Acquisition

Within the permit area, we aimed to measure areas that were most like the lunar terrain and also had the potential to form spots of frost. We searched for broad areas with a generally rocky texture, little to no organic materials, and slopes low enough to be accessible by a rover. Within those locations, we used different strategies to choose individual spots to measure: in a large open area between two cinder cones, we took samples at approximately regular intervals, first following a spiral pattern out from a central starting spot, then switching to a more linear path while maintaining a similar grid of targets. The goal of this strategy was to get relative coverage of the entire location and capture variations within it (see Figure 8 a) and Figure 9). Then inside

one of the cinder cones, we followed a more ad hoc strategy, choosing spots to sample by searching for unique features, such as variations in particle size, color, and texture (see Figure 9 and Figure 10). We also looked for spots that were likely to spend more time in shadow and thus be more likely to harbor frost, such as under overhanging rocks or between two rocks leaning against each other (Figure 11). In a few spots, we dug down just enough to reveal lower layers of the terrain which were different in color and/or texture than the surface layer (Figure 12). The distribution of the spots sampled in this location is visible in Figure 8 b).

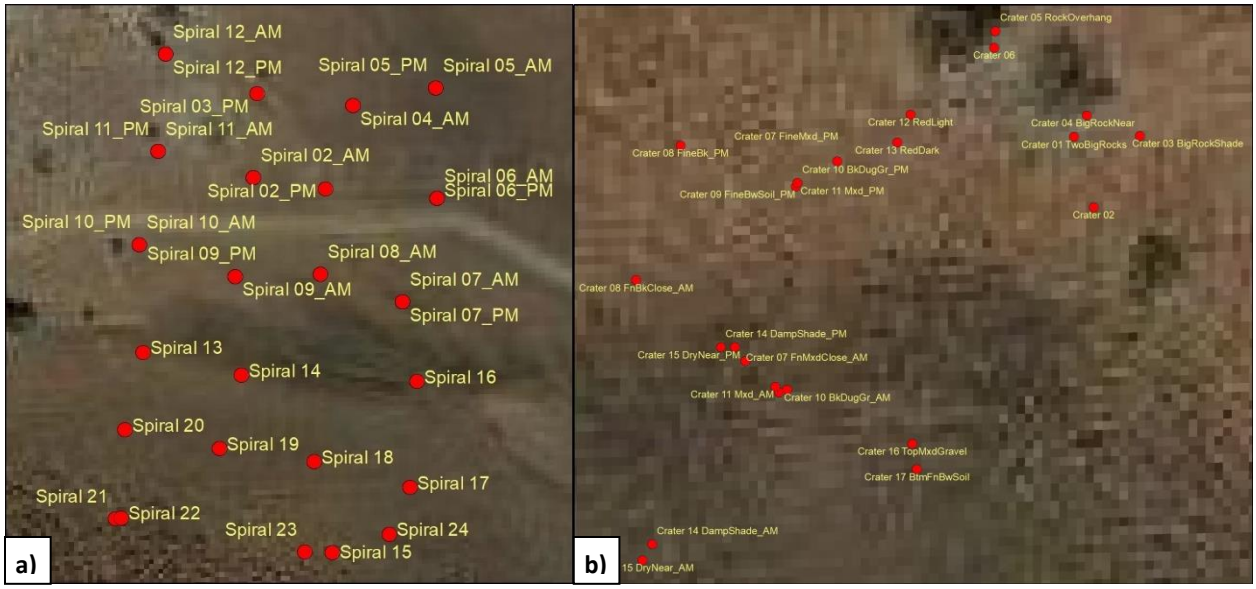

Figure 8: Sample spots chosen a) in a spiral/grid pattern and b) ad hoc

Figure 9: Operators conduct white reference calibration before sampling a spot with strong variations in color in the location between two cinder cones

Figure 10: Lighter and Darker Red rocks

Figure 11: Sample spot located in shadowed area between large rocks.

Figure 12: Sample spots which were dug up to measure lower layers of terrain.

For each measurement, the operator positioned the Sensor Staff such that the pistol grip pointed the fiber optic cable straight down at the target. Then a second operator placed the white reference staff such that the white reference panel was suspended between the fiber optic cable and the target (these positions are visible in Figure 9). On the operating computer, I ran the Optimization and White Reference operations within the ASD software until I could verify that the spectrum on the display showed a stable reflectance signal of approximately 1.0 (Figure 13).

Changes in cloud cover or other disruptions during this process could necessitate repeating one or both operations several times. Once a satisfactory white reference signal was achieved, the second operator removed the panel out from underneath the cable by either rotating the second staff or removing it completely, moving carefully so as not to bump the sensor and disrupt the signal (Figure 14). The operator waited a few seconds for the spectral signal to stabilize, then finally saved the measurement, saving at least two files for redundancy (Figure 15). The detailed step-by-step procedure followed for all data is in Table 2 in the Appendix.

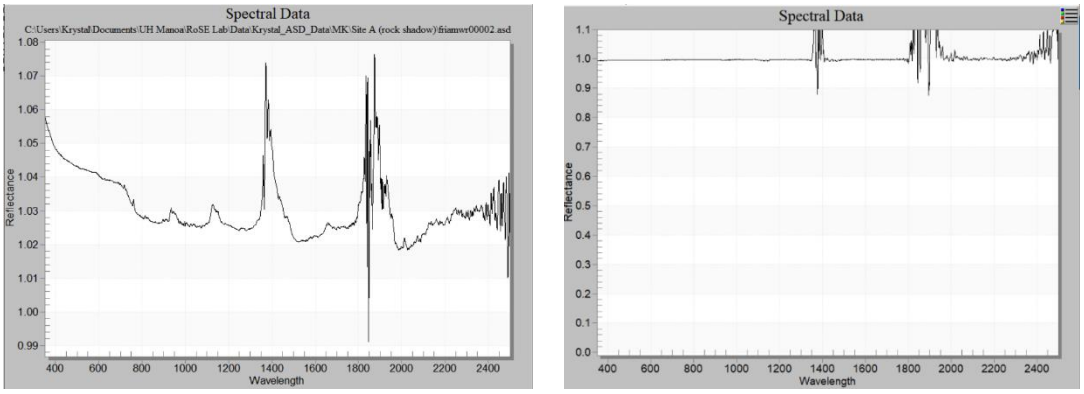

Figure 13: White Reference measurements taken in the field: Bad quality (L), Calibrated (R).

Over three days at the field site, we identified samples in four general locations: (1) by a trail near the power station, (2) in an open area between two cinder cones, (3) inside a cinder cone, and (4) on the outside slope of the cinder cone (spots at these locations are labeled with the prefixes ‘PS,’ ‘Spiral,’ ‘Crater,’ and ‘Slope,’ respectively, in Figure 16). While we were restricted to sampling in daylight hours due to using the sun as our spectrometer light source, we avoided sampling within the hours immediately before and after local noon when the sun would be most directly overhead. Instead, we conducted sampling sessions either in the morning just after dawn or in the evening just before dusk, when the position of the sun would result in greater phase angles and consequently greater levels of reflectance (De Castro & Li, 2023).

Figure 14: Positions of the field operators, Sensor Staff, and White Reference Staff during a field measurement.

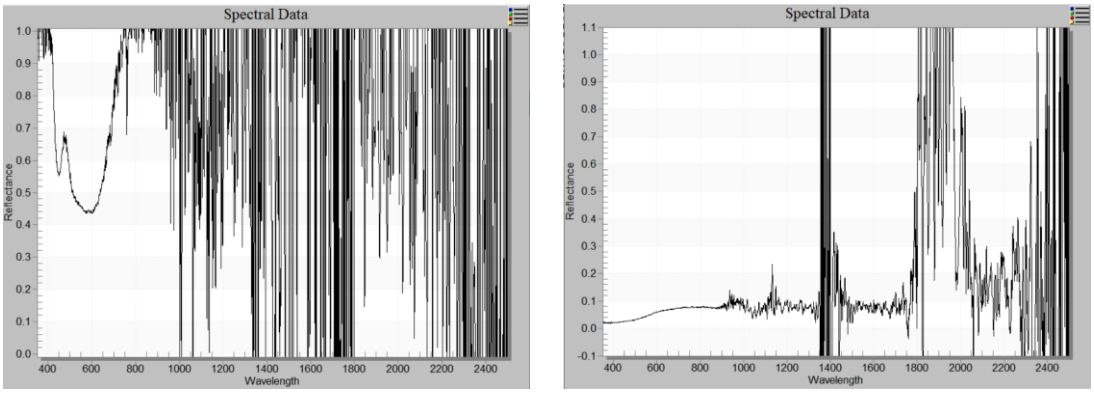

Figure 15: Spectral measurements taken in the field: Unstable (L), Stable (R).

Local temperatures were also cooler at these times of day; sampling in the morning gave us a greater chance of encountering frost that might have formed overnight before it could be melted or evaporated by the sun's heat. For this reason, some spots that we identified during the evening sessions as likely to get more shadow were revisited the following morning in hopes that any presence of water or ice would be more apparent when comparing the measurements against each other. In total, 48 unique spots were sampled, and 25 of those were sampled a second time during a morning session, resulting in 73 distinct sampling instances of 2 – 9 individually saved measurements each.

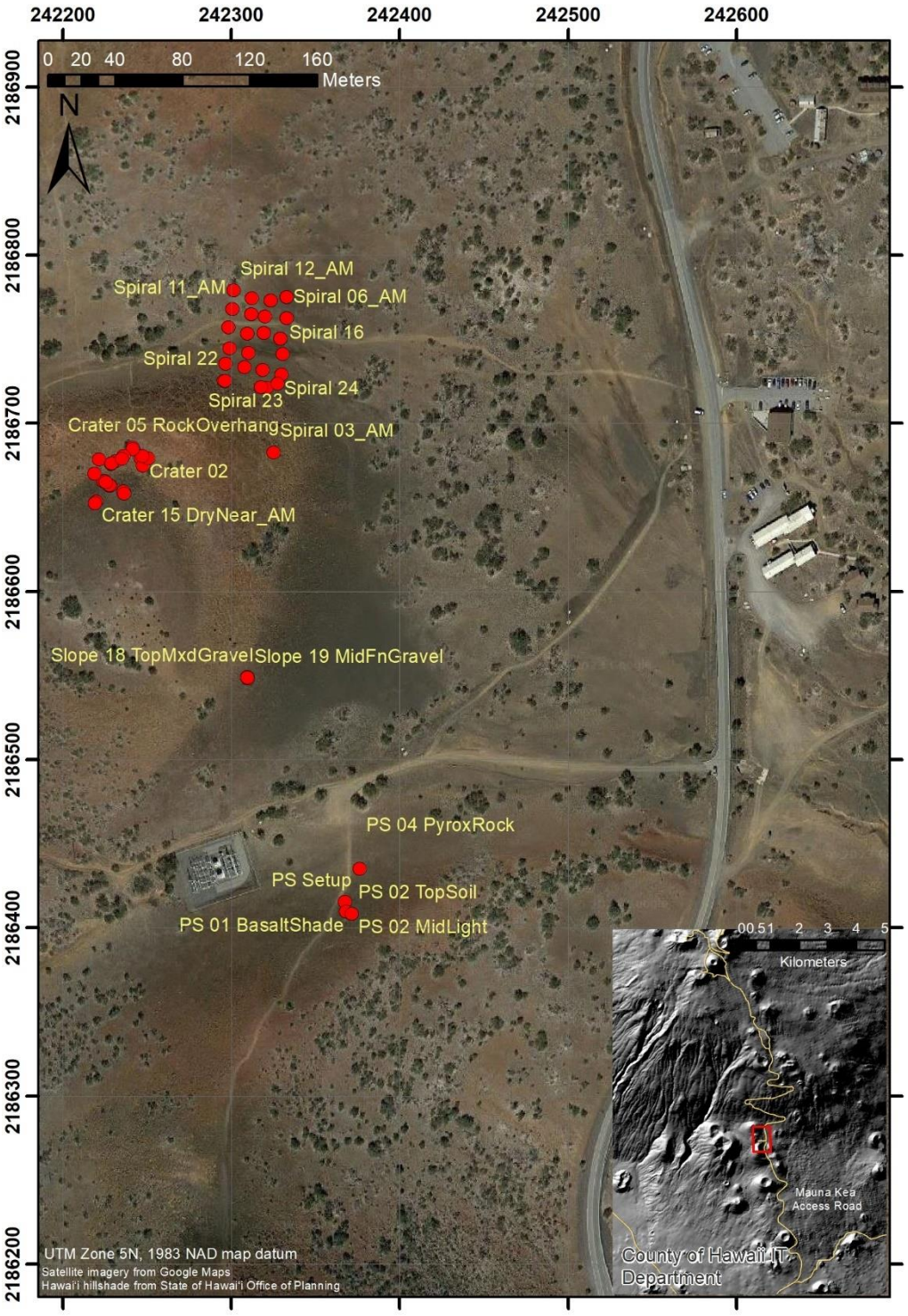

Figure 16: Sampling Sites on Mauna Kea: The four broad areas are differentiated by unique label prefixes among the clusters of coordinate points. The location of the research area lies along the Mauna Kea Access Road and is outlined in red in the inset.

2.4. Data Analysis

The data gathered in this campaign was processed and analyzed using a combination of ASD-provided software, Microsoft Excel, and original Python code. Each spectral measurement saved is stored by the spectrometer on the operational laptop as an individual *.asd* file, which is a binary format that is standard to ASD spectrometers and only readable by ASD software. Consequently, all processing steps between saving the spectral files and exporting the data as text files must be completed using the ASD processing software, ViewSpec Pro (*ViewSpec Pro User Manual*, 2008). The flowchart in Figure 17 illustrates these steps for an example spot with three individual files.

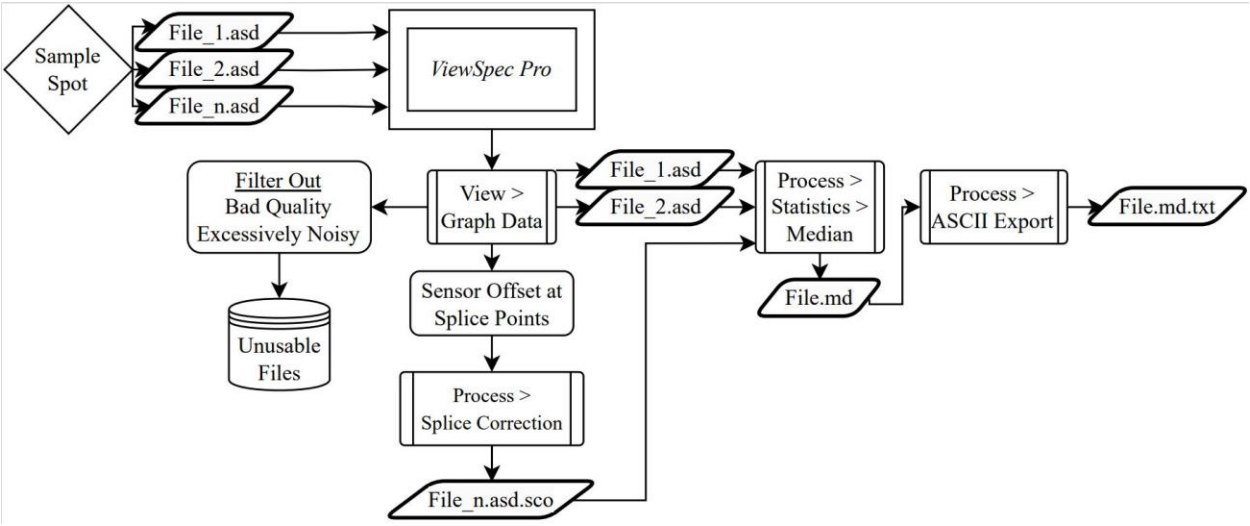

Figure 17: Spectrometer File Processing Flowchart.

The first step in processing the field data is to import all of the spectrometer *.asd* files into ViewSpec Pro and use the integrated graphing tool to perform an initial filter of the individual spectra by visually inspecting them. Any files which were of bad quality or excessively noisy were marked as unusable and discarded. Such files included those that were saved accidentally, those that contained unstable signals due to mid-measurement human error or changing

conditions, and those with atmospheric noise levels so high that they masked any underlying signal. Once all unusable data files are discarded, the remaining spectra are individually inspected for offsets at known splice points and corrected if necessary. This type of error is a result of the structure of VNIR spectrometers, which use three separate detectors to cover the full VNIR wavelength range and so are prone to offsets at the wavelengths where the mid-range detector overlaps each of the others (*FieldSpec 4 User Manual*, 2016). Every spectrum found to have this issue was corrected using ViewSpec Pro's Splice Correction tool, which outputs the corrected file with a slightly different extension (*.asd.sco*). After all of the files for the same unique sampling instant are checked, the *.asd* or *.asd.sco* files are combined into a single file with ViewSpec Pro's Statistics tool, which outputs the median signal of the group of spectra in a file with the extension *.md*. Combining the files this way can reduce the impact of errors or noise present in the individual measurements, and also reduces the total number of data files to process. Using the Median calculation rather than the Mean can reduce the impact on the combined signal of outlier values in the files, if any are present. The final step in processing the data files is converting them from the binary ASD format into ASCII text files with ViewSpec Pro's ASCII Export tool. This operation converts *.asd*, *.asd.sco*, and *.md* files to the much more common *.txt* format and offers several configuration options, such as setting the data format (relative Reflectance is the standard for these measurements), including header information, and specifying the field separator.

Analysis of the processed files was done using python code in a Jupyter Notebook framework. This code imports all of the text files into a pandas DataFrame, which easily holds the large amount of reflectance data due to all of the spectrometer files sharing the same wavelength range and values: the dataframe format uses one shared index for wavelength and

stores each file's reflectance values in a separate column. While files with excessive amounts of noise (such as the one displayed in Figure 19 a)) were already discarded, the remaining field data is still affected by atmospheric noise and must undergo a noise elimination process. This is a standard practice in spectroscopy which discards the reflectance values around the wavelength bands known to receive noise from atmospheric moisture: 1400 nm, 1800 nm, and 1900 nm. I first plotted all of the spectra and verified that the highest levels of noise occurred around these bands (see Figure 18 and Figure 19 b)), and then eliminated the rows in the dataframe corresponding to the wavelengths [1350:1460] and [1790:1960], which are the band boundaries commonly used by noise handling functions in spectral analysis toolboxes (Robinson & MacArthur, 2011). I also eliminated the last 100 rows corresponding to [2400:2500], which were consistently noisy across all files as well. I then re-plotted all of the spectra to verify successful deletion (Figure 19 c)).

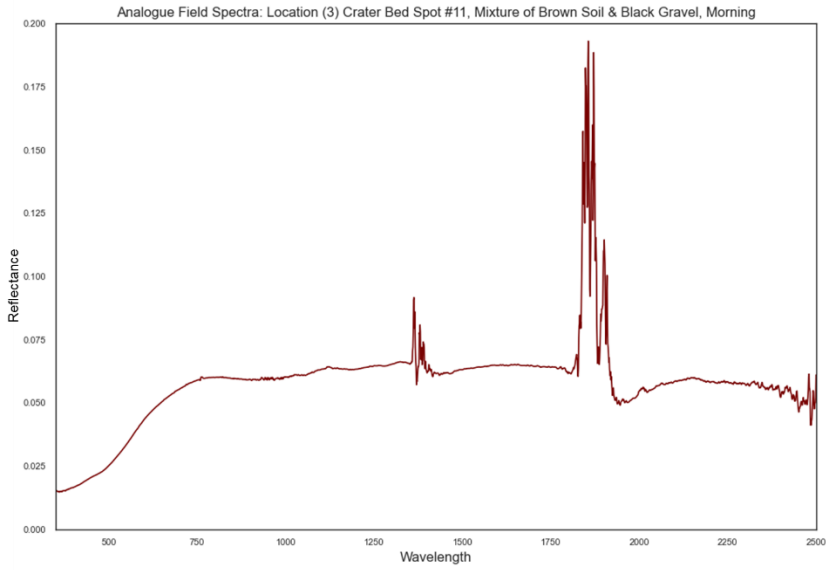

Figure 18: Plot of single spectrum with atmospheric water noise at 1400 nm and 1900 nm.

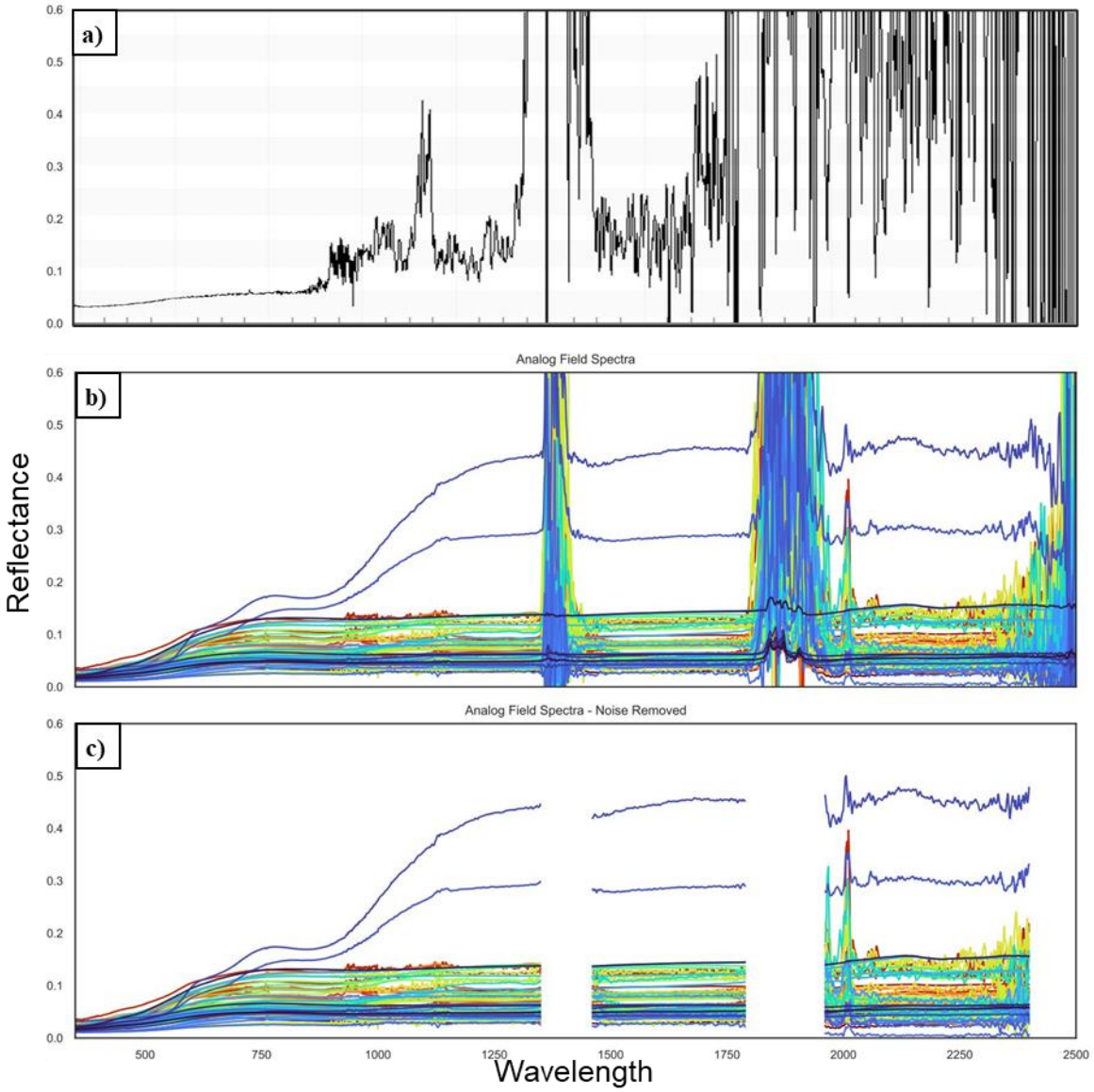

Figure 19: Analogue Field Data: a) Excessively noisy spectrum (Unusable), b) All field spectra, c) All field spectra with atmospheric water bands removed.

Because each spectral signal is a reflection of the geologic makeup of the measured target, comparing one spectrum to another gives an indication of the geologic similarity between those two targets. To quantify this similarity, we calculate the Pearson correlation coefficient between pairs of spectra, which results in a value from -1 to 1 (Bakeev & Chimenti, 2013; Henschel et al., 2020; Henschel & van der Spoel, 2020; Imai et al., 2002). A coefficient of 1 indicates a positive linear relationship between the two variables, meaning that the spectral signals have the same

shape, and therefore the targets can be assumed to have the same composition. Smaller correlation coefficients correspond to less similarity, with values of 0 and below indicating no similarity between the spectra. The pandas package has a built-in function (corr()) which calculates the pairwise Pearson correlation of the columns in a dataframe and returns a correlation matrix. In this matrix, each of the dataframe variables is listed as both a row and a column, such that the value at the intersection of each (row, column) pair is the correlation coefficient between those two variables. For a correlation matrix of spectral data, visualization as a heatmap provides an intuitive illustration of the similarity distribution, with either end of the chosen color bar corresponding to the extremes of no similarity and perfect equality, and all other values falling along the gradient between them. The heatmaps for this project were generated using the seaborn package.

Determining the analogue field site's geologic similarity to the lunar surface requires that the field data be compared to reference data representing the expected composition of the lunar regolith. For this reference data, we selected spectra of both lunar simulants and returned lunar samples, all of which are publicly available in the RELAB Spectral Database (Milliken, 2020) and USGS Spectral Library Version 7 (Kokaly et al., 2017) planetary science databases. The files were chosen based on current knowledge of the lunar South Pole environment, which is located in the southern highlands and dominated by anorthosite (Gawronska et al., 2020; Spudis et al., 2008; Wilhelms et al., 1979). Consequently, the files used include highland samples from the Apollo 14 and 16 missions, highland simulants, and anorthositic simulants. We also included some mare and basaltic simulants and samples from other Apollo missions for comparison. Due to their having originated from multiple sources, these files contained various wavelength ranges, so the data in each file had to be matched to the standard spectrometer wavelength values upon

being imported into the dataframe format. Once the shared wavelength index matches that of the field data dataframe, the two can be combined into a single dataframe, and a correlation matrix generated for all of the data files. From this robust matrix, I extracted the segments containing unique pairs of the field data files and the reference data files, creating a sub-matrix and corresponding heatmap for the field data compared with the simulants, and another sub-matrix and heatmap for the field data compared with the returned samples. The flowchart in Figure 20 illustrates the steps in the code used to generate the different correlation coefficient heatmaps.

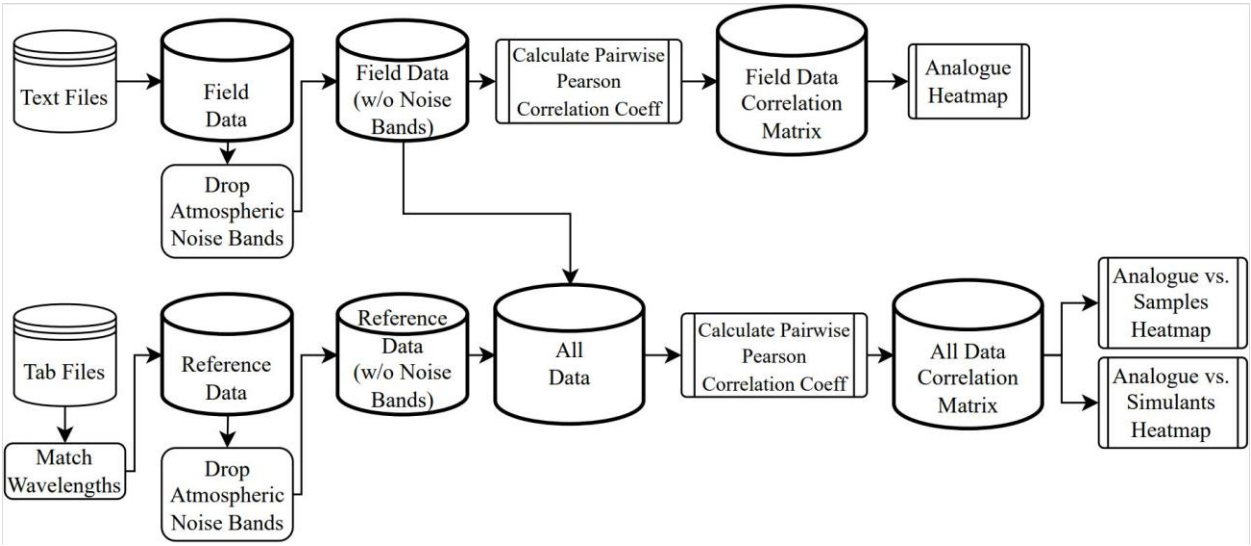

Figure 20: Data Analysis Flowchart.

3. RESULTS

Analysis of the data gathered during this field campaign resulted in three heatmaps visualizing the correlation coefficients between pairs of spectra as described in the section above. Lighter colored cells indicate less similarity and darker colors indicate higher similarity, as shown by the color bar next to each figure. Expanded descriptions of each sample file are listed next to their figure labels in Table 1 in Appendix A. The correlation matrix for the analogue field data is shown in Figure 21. This matrix illustrates the geologic similarity within the field site, as

it is composed of the correlation coefficients between each pair of sample spots. Darker shades dominate the figure, indicating a high amount of geologic similarity among the samples,

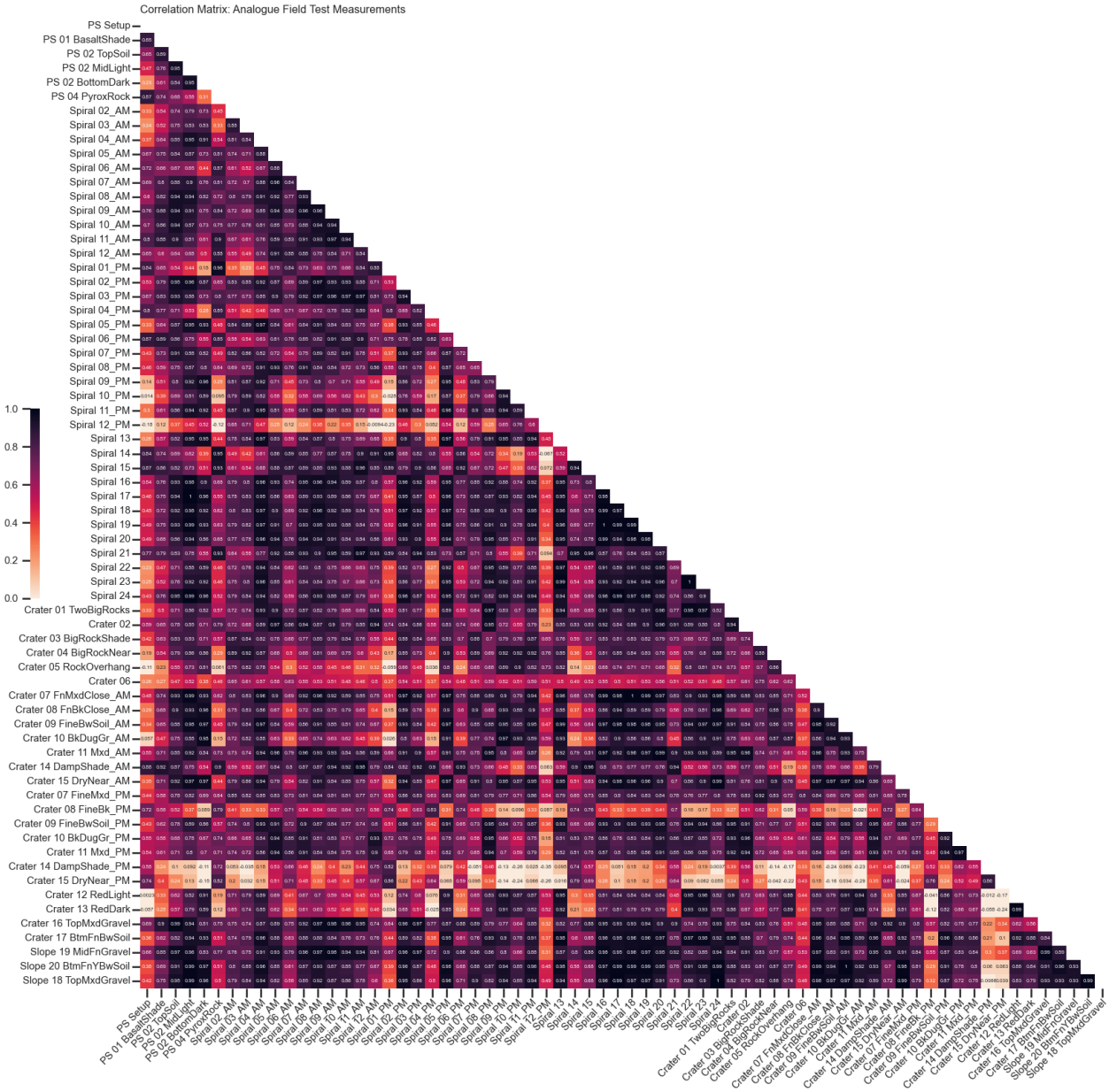

Figure 21: Correlation matrix: Analogue Field Samples

with a few lighter-colored rows and columns sticking out as dissimilar outliers. Although it is clear that there is variation among all of the field spectra, we can conclude from this initial overview that the field site is generally geologically consistent.

The sub-matrix with the correlations between the field data and the simulants is shown in Figure 22. This matrix has multiple rows and columns dominated by very light colors, indicating a strong dissimilarity among those files. The lightest rows correspond to multiple highland simulants – which we had expected to have a higher correlation with the field samples – as well as a couple of the mare simulants. The rows with the darkest shades and therefore the highest similarity correspond to the anorthositic simulants, followed by the basaltic simulants.

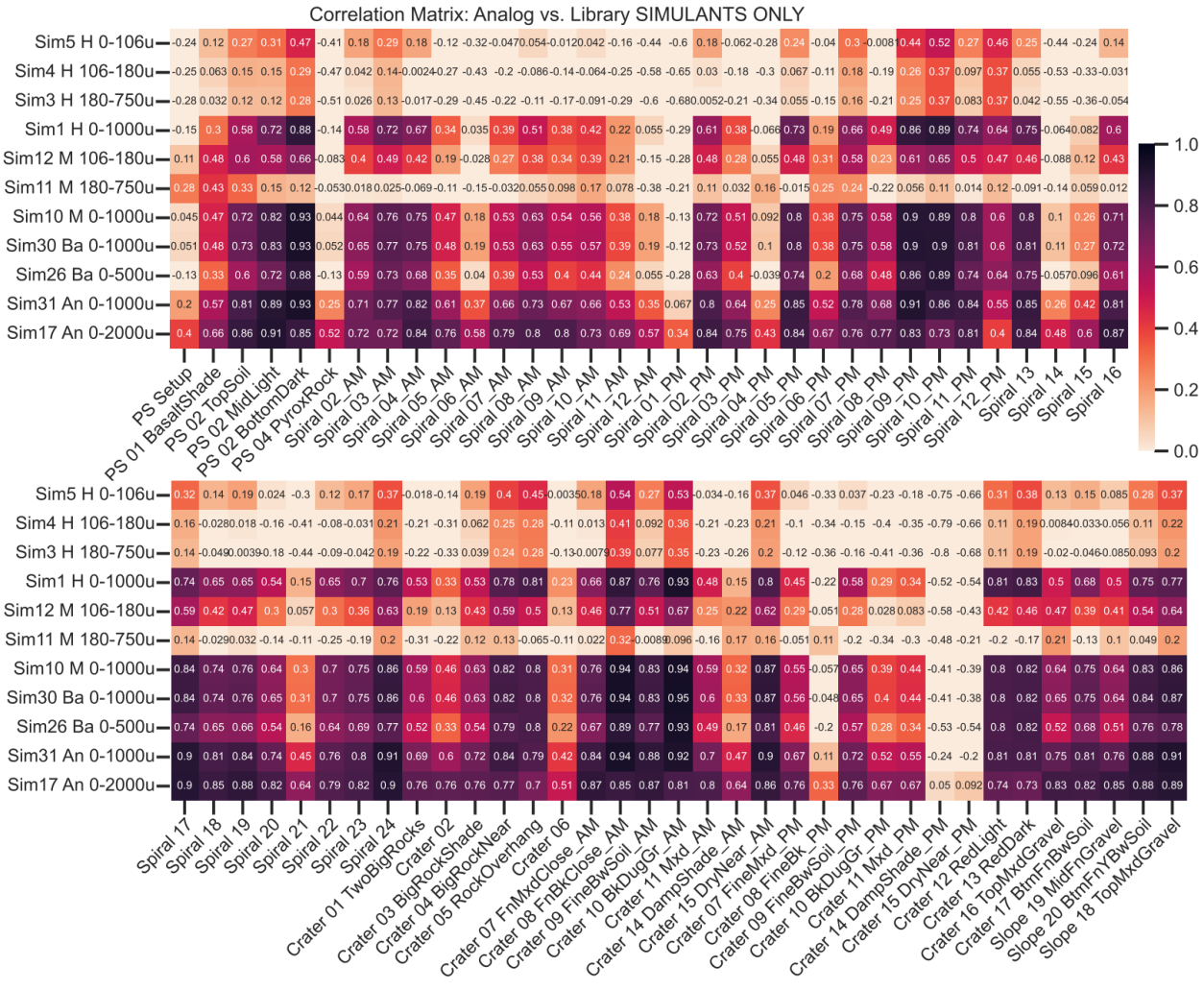

Figure 22: Correlation matrix: Analogue Samples and Lunar Simulants

The sub-matrix with the correlations between the field data and the returned lunar samples is shown in Figure 23. While this matrix shows multiple columns and a few rows with very light

colors resulting from very low levels of similarity, the majority of the correlation values indicate strong similarity, especially with the Apollo 16 highland and Apollo 11 mare samples.

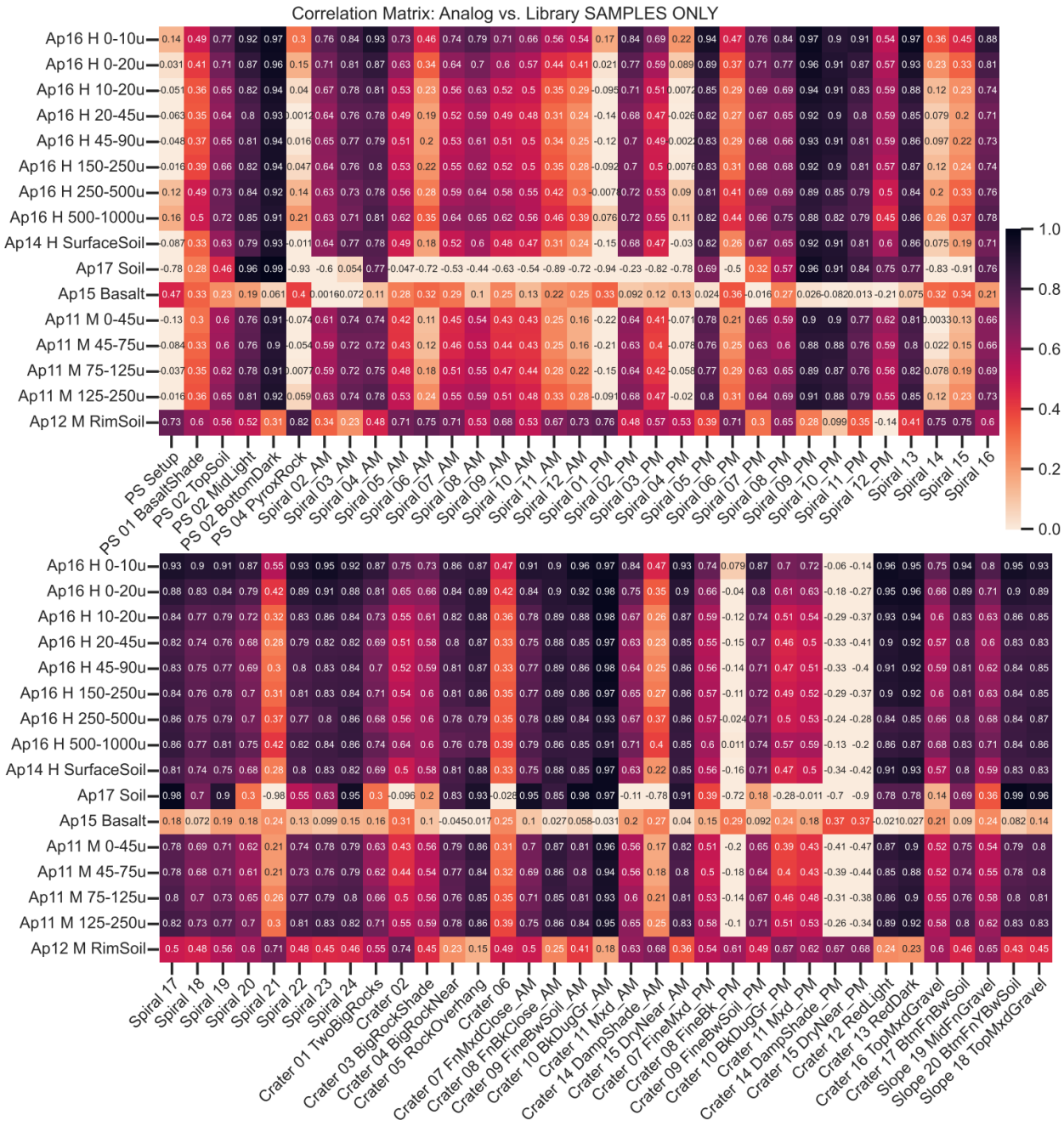

Figure 23: Correlation of Analogue Samples and Lunar Samples

4. DISCUSSION

The sensor suite and data acquisition method described in this report were successfully used to collect reflectance data from the field site, although it did not go entirely as planned. The biggest issue that we had during the data-gathering trip was that we were unable to collect measurements of water ice because we did not encounter any while selecting targets. This was likely due to a few different factors that affected the ground temperature of the field site and prevented it from dropping low enough to form frost: the dates of the trip were in early April, when the seasonal temperature was already on the rise; the permit limited us to the ~9200-ft-elevation research zone, while higher areas on Mauna Kea still had snow on the ground; and the use of the sun as our light source limited us to daytime measurements, rather than being able to take advantage of the cooler temperatures overnight. Consequently, we were not able to validate the mission requirement for the field site to be capable of experiencing scattered ice distribution, nor could we derive any feedback on our ability to detect water ice in the spectral data.

However, we were able to use the data analysis method with the gathered spectral data to investigate the validity of the field site as a geologic analogue for the lunar surface. Although measurements of South Pole regolith samples do not yet exist, the geology is expected to be similar to that of samples returned by the Apollo missions, so we used that publicly available reflectance data as our ground truth for comparison. We also used reflectance data of various lunar simulants which emulate particular properties of lunar regolith. Comparison of the field data to this reference data resulted in a variety of correlation coefficients, as seen in Figure 22 and Figure 23. For the simulant data, the greatest factor that appeared to influence spectral similarity was not highland vs. mare or anorthosite vs. basalt as expected, but rather particle size: the rows with the lightest colors and therefore lowest correlation coefficients with most of the

field spots all correspond to the simulants with the smallest sizes (< 750 μm). Conversely, the rows for the simulants with particle sizes up to 1000–2000 μm are much darker, with high correlation coefficients in the 0.70-0.95 range. We can conclude from this pattern that the field site is more analogous to lunar regolith that is composed of larger particles. In the returned samples heatmap, the visible vertical stripe pattern indicates that most of the Apollo samples are highly correlated with each other, as they produced very similar correlation coefficients with each field sample. We can see that certain field samples have very low correlation with the Apollo samples, but the majority of the field spots produced very high correlation coefficients instead, again in the range of 0.70 and above, even reaching as high as 0.99. Notably, the returned samples with which the field site had the lowest similarities were the two from Apollo 12 and Apollo 15, while the samples from Apollo 11, 14, and 16 all produced similarly high correlation coefficients regardless of their particle size. Another interesting note is that the field spots with consistently highest correlation coefficients across both the simulants and the returned samples were those where the surface layer was dug up to access and measure the lower layers of soil. With the vast majority of the field data showing strong similarity to the majority of the reference data – especially to the returned samples – we can conclude that the analogue field site is sufficiently geologically similar to the lunar surface to validate it as a lunar surface analogue.

We also wanted to confirm that the geology of the analogue field site is relatively consistent, such that its similarity to the lunar surface is not limited to specific locations but rather extends throughout the area. By looking at the heatmap for the field data in Figure 21, we can see that the majority of the correlation coefficients are darkly shaded with values of 0.60 and above, indicating that they are mostly very similar in composition. As an additional check, we investigated whether any relationship exists between the distance separating two spots and their

correlation coefficient. For this check, I used the GPS location data recorded for each sample to calculate the geographical distance between each pair of spots. I then imported these distances to the data analysis code and linked each pair's distance to their correlation coefficient from the field data correlation matrix. Finally, I created a scatterplot of all of the (distance, correlation coefficient) pairs, as seen in Figure 24. It is immediately apparent from the scatterplot that no

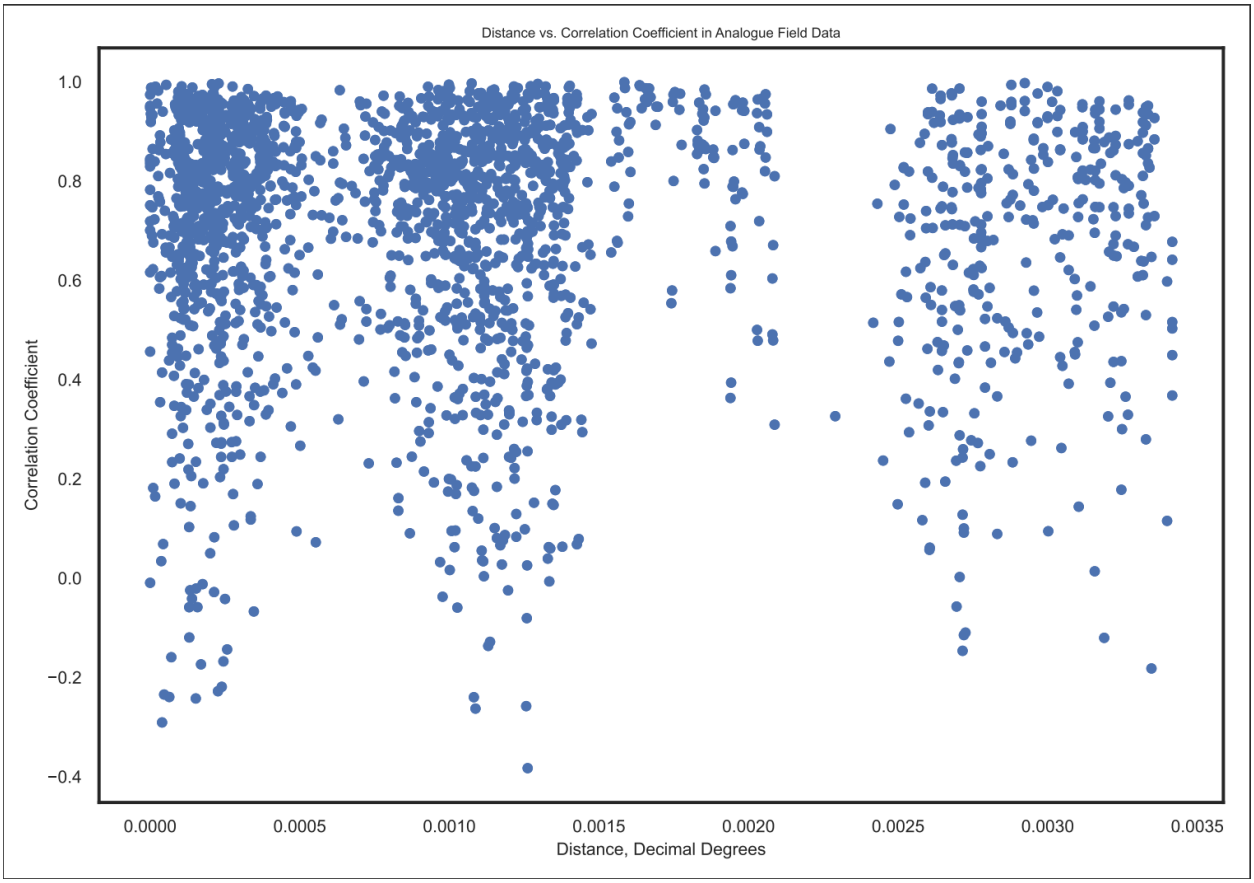

Figure 24: Geographical Distance vs. Correlation Coefficient scatter plot among Analogue Field Site Samples

strong linear relationship exists between geographical distance and spectral similarity, although the two dense point clusters in the top left of the plot suggest that many pairs of spots with highly similar spectral signals are located relatively close to each other. The distribution of the

scatterplot also shows that the majority of the correlation coefficients fall in the top section (around 0.60 and above), confirming the high levels of similarity among the sample spots.

5. CONCLUSION

For this project, I developed an experiment campaign to validate the Pu‘uhaiwahine field site as a lunar surface analogue that can be used to test an ice-prospecting rover’s exploration strategy. I designed and built a human-operated sensor suite to use to gather VNIR reflectance data of the field site terrain, and completed my first data-gathering trip to Mauna Kea in April 2023. I then used the campaign data analysis flow to process and analyze all of the field data, comparing it against ground truth lunar reference data. The reference data consisted of reflectance data from various lunar simulants and returned samples from the Apollo missions. To compare the spectral signatures from the field site to that of the reference data, I generated three heatmaps, each visualizing a different correlation matrix: the field data’s correlation matrix with itself, the field data’s correlation matrix with the lunar simulants, and the field data’s correlation matrix with the returned samples. The results illustrated in the heatmaps and discussed in the previous section indicate that the vast majority of the field data shows a strong similarity to the majority of the reference data, especially to the returned samples, and that the spectral characteristics in the field data are relatively consistent throughout the entire field site. From these results, we can conclude that the analogue field site is sufficiently geologically similar to the lunar surface to validate it as a lunar surface analogue.

Besides having sufficient geologic similarity to the expected lunar regolith, however, to qualify as a useful planetary analogue specifically for the ice-prospecting rover’s future performance tests, the field site must also meet the second requirement, which is to have terrain that is capable of forming a scattered distribution of detectable water ice. Unfortunately, the team

did not locate any instances of water ice within the permitted research zone while selecting sampling targets, so we were unable to validate this second requirement, nor were we able to use and evaluate our analysis procedures to detect water ice in the spectral data. Consequently, a key goal of the next data-gathering trip to Mauna Kea will be to locate and measure instances of water ice, which is why the permit submitted to the DLNR DOFW for a second trip requests an expansion to the previous research zone (see map in Appendix D). The new proposed area would include the land immediately alongside the road, where we could expect to find snow piled up after it has been plowed off of the road, as well as a larger, more open area with shallow slopes where the rover would have space to maneuver, and which is located at a higher elevation and thus improves our chances of encountering ice. Additionally, the dataset from this report will be able to be used as high-fidelity reference data or ground truth for the analogue site, increasing the likelihood that we will be able to detect the added presence of ice in the relevant spectra. Other improvements for future field trips include a switch to an active light source for the spectrometer rather than relying on sunlight, which would both minimize effects from changing environmental light conditions and give us the ability to conduct measurements at night, and using the rover-mounted configuration of the sensor suite, so that human operational errors are reduced and we can test the performance of the rover's path planning and exploration strategy algorithms.

Despite not getting to use it to detect the presence of water ice at the field site, this experiment campaign succeeded in gathering and analyzing data from the prospective analogue field site as intended. Therefore, we can conclude that it is an effective method for taking spectral measurements of a desired field site, comparing them to selected reference data, and using the level of similarity between them to validate the field site as a planetary analogue for the mission.

Appendix A

Table 1 Analogue Field and Reference Library Data Name Codes and Descriptions

LABEL	DESCRIPTION
Analogue Field Data	
'PSxxx'	**Location (1) Power Station**
PS Setup	Setup Area
PS 01 BasaltShade	Spot #01, Basalt, Shade under rock
PS 02 TopSoil	Spot #02, Soil Layers - Top
PS 02 MidLight	Spot #02, Soil Layers - Middle, Light-colored
PS 02 BottomDark	Spot #02, Soil Layers - Bottom, Dark-colored
PS 04 PyroxRock	Spot #04 Rock, Pyroxene Xenolith
'Spiralxxx'	**Location (2) Between Two Cinder Cones**
Spiral 02_AM	Spot #02, Spiral Pattern, Morning
Spiral 03_AM	Spot #03, Spiral Pattern, Morning
Spiral 04_AM	Spot #04, Spiral Pattern, Morning
Spiral 05_AM	Spot #05, Spiral Pattern, Morning
Spiral 06_AM	Spot #06, Spiral Pattern, Morning
Spiral 07_AM	Spot #07, Spiral Pattern, Morning
Spiral 08_AM	Spot #08, Spiral Pattern, Morning
Spiral 09_AM	Spot #09, Spiral Pattern, Morning
Spiral 10_AM	Spot #10, Spiral Pattern, Morning
Spiral 11_AM	Spot #11, Spiral Pattern, Morning
Spiral 12_AM	Spot #12, Spiral Pattern, Morning
Spiral 01_PM	Spot #01, Spiral Pattern, Dusk
Spiral 02_PM	Spot #02, Spiral Pattern, Dusk
Spiral 03_PM	Spot #03, Spiral Pattern, Dusk
Spiral 04_PM	Spot #04, Spiral Pattern, Dusk
Spiral 05_PM	Spot #05, Spiral Pattern, Dusk
Spiral 06_PM	Spot #06, Spiral Pattern, Dusk
Spiral 07_PM	Spot #07, Spiral Pattern, Dusk
Spiral 08_PM	Spot #08, Spiral Pattern, Dusk
Spiral 09_PM	Spot #09, Spiral Pattern, Dusk
Spiral 10_PM	Spot #10, Spiral Pattern, Dusk
Spiral 11_PM	Spot #11, Spiral Pattern, Dusk
Spiral 12_PM	Spot #12, Spiral Pattern, Dusk
Spiral 13	Spot #13, Grid Pattern
Spiral 14	Spot #14, Grid Pattern
Spiral 15	Spot #15, Grid Pattern
Spiral 16	Spot #16, Grid Pattern
Spiral 17	Spot #17, Grid Pattern
Spiral 18	Spot #18, Grid Pattern

Spiral 19	Spot #19, Grid Pattern
Spiral 20	Spot #20, Grid Pattern
Spiral 21	Spot #21, Grid Pattern
Spiral 22	Spot #22, Grid Pattern
Spiral 23	Spot #23, Grid Pattern
Spiral 24	Spot #24, Grid Pattern
'Craterxxx'	**Location (3) Crater Bed**
Crater 01 TwoBigRocks	Spot #01, Between Two Big Rocks
Crater 02	Spot #02
Crater 03 BigRockShade	Spot #03, Under Big Rock, Shaded
Crater 04 BigRockNear	Spot #04, Near Big Rock, Open Area
Crater 05 RockOverhang	Spot #05, Under a Rock Overhang
Crater 06	Spot #06
Crater 07 FnMxdClose_AM	Spot #07, Fine Sand, Mixed Brown/Black, Similar nearby to original #07, Morning
Crater 08 FnBkClose_AM	Spot #08, Fine Sand, Black, Nearby location to original #08, Morning
Crater 09 FineBwSoil_AM	Spot #09, Fine Brown Soil Dug from Under Top Gravel, Morning
Crater 10 BkDugGr_AM	Spot #10, Very Black Gravel Dug from Under Brown Soil, Morning
Crater 11 Mxd_AM	Spot #11, Mixture of Brown Soil & Black Gravel (#10 & #11), Morning
Crater 14 DampShade_AM	Spot #14, Damp Soil Under Rock Overhang, Morning
Crater 15 DryNear_AM	Spot #15, Dry Soil of Similar Color Near #14 Damp Soil, Morning
Crater 07 FineMxd_PM	Spot #07, Fine Sand, Mixed Brown/Black, Dusk
Crater 08 FineBk_PM	Spot #08, Fine Sand, Black, Dusk
Crater 09 FineBwSoil_PM	Spot #09, Fine Brown Soil Dug from Under Top Gravel, Dusk
Crater 10 BkDugGr_PM	Spot #10, Very Black Gravel Dug from Under Brown Soil, Dusk
Crater 11 Mxd_PM	Spot #11, Mixture of Brown Soil & Black Gravel (#10 & #11), Dusk
Crater 14 DampShade_PM	Spot #14, Damp Soil Under Rock Overhang, Dusk
Crater 15 DryNear_PM	Spot #15, Dry Soil of Similar Color Near #14 Damp Soil, Dusk
Crater 12 RedLight	Spot #12, Red Rock 1, Lighter
Crater 13 RedDark	Spot #13, Red Rock 2, Darker
Crater 16 TopMxdGravel	Spot #16, Upper Layer, Mixed Gravel
Crater 17 BtmFnBwSoil	Spot #17, Bottom Layer, Brown Fine Soil
'Slopexxx'	**Location (4) Crater Side**
Slope 19 MidFnGravel	Spot #19, Middle Layer, Finer Gravel
Slope 20 BtmFnYBwSoil	Spot #20, Bottom Layer, Fine Soil, Light-colored (Yellow/Brown)
Slope 18 TopMxdGravel	Spot #18, Top Layer, Top Mixed Gravel
Reference Library Data	
Sim5 H 0-106u	Simulant #5, Highland, 0-106um
Sim4 H 106-180u	Simulant #4, Highland, 106-180um
Sim3 H 180-750u	Simulant #3 Highland, 180-750um
Sim1 H 0-1000u	Simulant #1, Highland, 0-1000um
Sim12 M 106-180u	Simulant #12, Mare, 106-180um
Sim11 M 180-750u	Simulant #11, Mare, 180-750um
Sim10 M 0-1000u	Simulant #10, Mare, 0-1000um

Sim30 Ba 0-1000u	Simulant #30, Basaltic, 0-1000um
Sim26 Ba 0-500u	Simulant #26, Basaltic, 0-500um
Sim31 An 0-1000u	Simulant #31, Anorthositic, 0-1000um
Sim17 An 0-2000u	Simulant #17, Anorthositic, 0-2000um
Ap16 H 0-10u	Apollo 16 Sample, Highland, 0-10um
Ap16 H 0-20u	Apollo 16 Sample, Highland, 0-20m
Ap16 H 10-20u	Apollo 16 Sample, Highland, 10-20m
Ap16 H 20-45u	Apollo 16 Sample, Highland, 20-45m
Ap16 H 45-90u	Apollo 16 Sample, Highland, 45-90m
Ap16 H 150-250u	Apollo 16 Sample, Highland, 150-250um
Ap16 H 250-500u	Apollo 16 Sample, Highland, 250-500um
Ap16 H 500-1000u	Apollo 16 Sample, Highland, 500-1000um
Ap14 H SurfaceSoil	Apollo 14 Sample, Highland, Surface Soil
Ap17 Soil	Apollo 17 Sample, Soil
Ap15 Basalt	Apollo 15 Sample, Basalt
Ap11 M 0-45u	Apollo 11 Sample, Mare, 0-45um
Ap11 M 45-75u	Apollo 11 Sample, Mare, 45-75um
Ap11 M 75-125u	Apollo 11 Sample, Mare, 75-125um
Ap11 M 125-250u	Apollo 11 Sample, Mare, 125-250um
Ap12 M RimSoil	Apollo 12 Sample, Mare, Crater Rim Soil

Appendix B

Table 2 Data Gathering Procedure

Step	*Description*
SETUP	
1) Power On Spectrometer	Connect charged field battery to the spectrometer and flip the Power Switch to ON. The spectrometer must warm up for a minimum of 20 minutes to stabilize its readings.
2) Connect Laptop	Connect the operational laptop to the instrument's internal wireless network to enable data transmission.
3) Launch Spectrometer Software	Start the RS3 High Contrast program and confirm network connection.
4) Power On Sensors	Connect the combined power and data cable from the Arduino UNO to the laptop. Verify power to the IMU and GPS via on-board LEDs. The GPS can take up to 20 minutes to calibrate its position after establishing line-of-sight.
5) Launch Sensor Software	Start Data Streamer in Excel, connect to the appropriate COM Port, and verify that sensor data is streaming.
SPECTRAL MEASUREMENT	
6) Configure Spectra Save Settings	Set the save folder and naming options in the RS3 Control settings.
7) Clean White Reference	Clean the white reference panel with compressed air if needed.
8) Position Optics	Place the sensor staff on the ground such that the spectrometer fiber optic cable points directly down at the target. The field operator should orient the staff and their own body such that neither blocks sunlight to the target.
9) Position White Reference	Place the white reference staff on the ground such that the panel is in between the fiber optic cable and the target, with the center of the panel centered under the cable aperture.
10) Optimization	Press the 'Opt' button in RS3 to perform Optimization and Dark Current measurements. Repeat if necessary.
11) White Reference Calibration	Press the 'WR' button in RS3 to perform calibration. Confirm appropriate spectrum on the on-screen display before proceeding. Repeat multiple times if necessary.
12) Remove White Reference Panel	Carefully rotate the panel out from underneath the spectrometer aperture without disturbing either the sensor staff or the target.
13) Wait for Stabilization	Allow the display to stabilize to a constant spectrum for the target.
14) Save Spectra	Set a new file save name if desired and save multiple consecutive spectra, allowing a couple of seconds between each.

Appendix C: Mauna Kea Field Test 1 DOFW Research Report

DOFW Permit for Access, Collecting, and Research – Report

Granted to: Christian Andersen (UH Hilo), Krystal Arroyo-Flores (UH Manoa), Paolo Espejo (UH Manoa), Hao Wang (UH Manoa), Frances Zhu (UH Manoa)
For: To quantify the presence of ice (frost) in the soil and to characterize the physical properties of the soil.
Location: Mauna Kea Forest Reserve
Period: March 10, 2023 – April 30, 2023 (Request filed February 16, 2023)

Report:

The research conducted under this permit was completed April 7-9, 2023, in the Pu'uhaiwahine valley on Mauna Kea. The research team used a portable Visible and Near-Infrared (VNIR) spectrometer to collect spectral measurements and a portable bevameter to collect sinkage data from various sample sites throughout the field site. These measurements were used to characterize the terrain and its physical properties, and to evaluate its likeness to the terrain of the lunar South Pole.

Sampling was conducted around Pu'uhaiwahine at four distinct areas, identified as Location (1) Power Station, Location (2) Between Two Cinder Cones, Location (3) Crater Bed, and Location (4) Crater Slope (see attached map). Individual spots in each area were selected according to either a physical sampling pattern (i.e. following a spiral or grid) or based on visual cues (e.g. color, particle size, suspected composition) to capture representative samples of the terrain. Measurements were taken either in the early morning or early evening to increase the likelihood of encountering frost due to lower temperatures, and some areas were sampled a second time to collect reflection data under different lighting conditions.

Analysis of the data gathered at the location was conducted mainly with python, with pre-processing of the spectral measurements conducted using ViewSpec Pro, which is a software application provided by the spectrometer manufacturer, Analytical Spectral Devices, Inc. The sinkage measurements collected with the bevameter were used to create pressure vs. sinkage datasets which could then be used to evaluate the accuracy of environmental simulations. The spectral measurements collected with the spectrometer were used to create datasets of relative reflectance according to location, which were then used to evaluate spectral consistency within the field site as well as similarity of the field site to existing lunar data (based on reflectance measurements of lunar samples and lunar simulants downloaded from public databases). Unfortunately, the team encountered no frost in the soil and so was unable to perform any analysis related to the presence of ice.

A paper on the analysis of the spectral measurements will be presented at the 2023 AIAA ASCEND conference in Las Vegas, Nevada, and will be provided to DOFW after publication. The spectral data collected will be published on GitHub with public access, accompanied by the photos of sampling sites and location information. The data and code will be available on GitHub at https://github.com/frankiezoo/hawaii_moon_analogue.

1

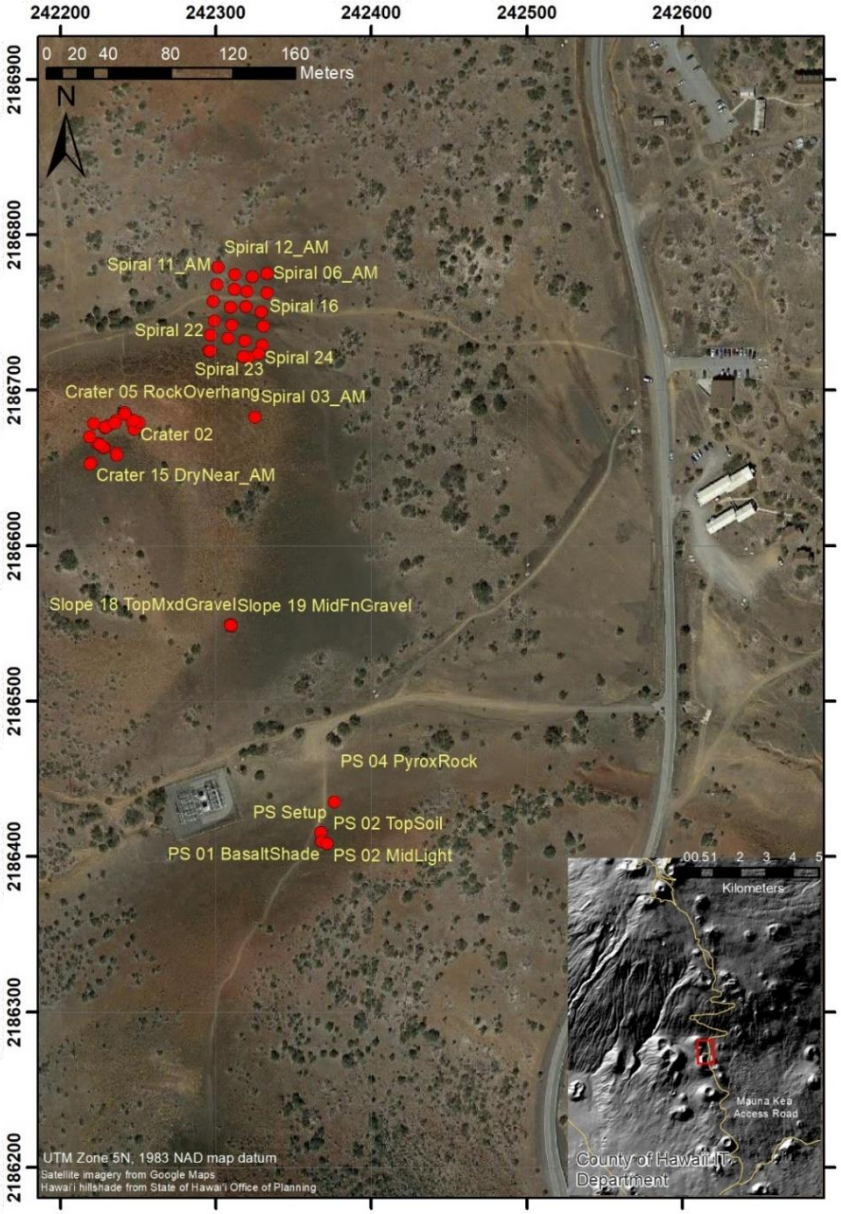

Sampling Sites on Mauna Kea. The location of the research area lies along the Mauna Kea Access Road and is outlined in red in the inset.

2

Appendix D: Areas Included in Permit Request for Field Trip 2

Reference Map

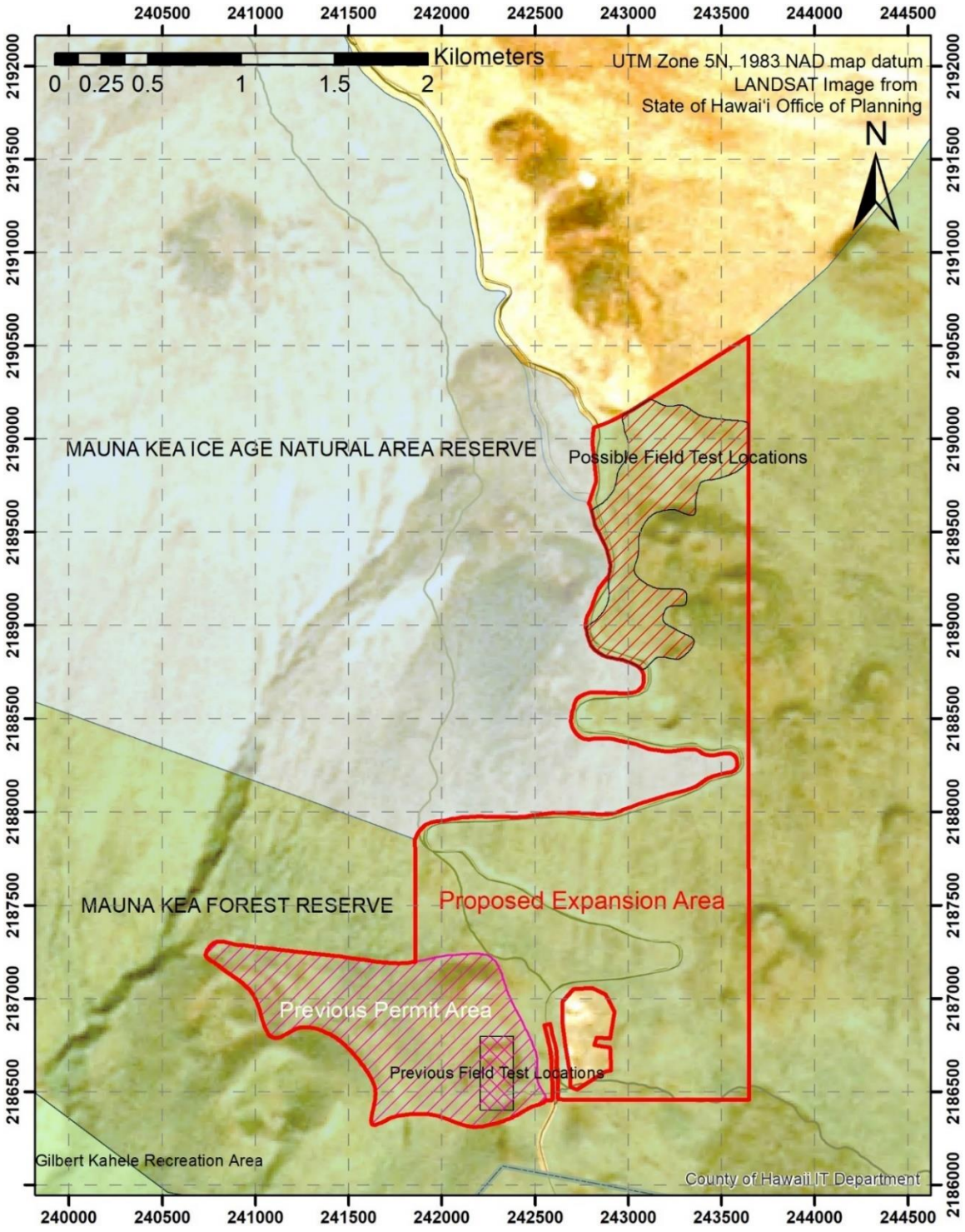

Area of interest for proposed research outlined in red (research area from previous permit outlined and shaded in pink). Additional area proposed is for mostly along Mauna Kea Access Road or lower Humu'ula Trail, plus low-slope area hatched in red.

Acknowledgments

First and foremost, I would like to thank my advisor, Dr. Frances Zhu, for the opportunity to work with her on this project, for her guidance and support, and for her endless patience and encouragement. Additionally, I would like to thank Dr. Hao Wang, Christian Andersen, Paolo Espejo, Christian Pak, and Nina de Castro for their assistance and key contributions to the success of the field trip, before, during, and after. I would also like to thank my committee member Dr. Shuai Li and his students in the HIGP Li Lab for their invaluable instruction, guidance, and flexibility, as well as my committee member Dr. Paul Lucey and his student, Elizabeth Fisher, for their interest in this project and additional spectrometer expertise. And lastly to my friends in the RoSE Lab for their biweekly excitement and encouragement for every update.

This project was supported by the NASA Established Program to Stimulate Competitive Research (EPSCoR) Grant HI-80NSSC21M0334 and the Hawai‘i Space Grant Consortium (HSGC). I would particularly like to thank the HSGC for their support of my Graduate Assistantship.

Open Research

The spectral measurements from this trip and future field tests will be published on GitHub with public access, along with any reference data used and the analysis code. These materials will be available at: https://github.com/frankiezoo/hawaii_moon_analogue.

References

Bakeev, K., & Chimenti, R. (2013). Pros and Cons of Using Correlation Versus Multivariate Algorithms for Material Identification via Handheld Spectroscopy. *American Pharmaceutical Review*. https://www.americanpharmaceuticalreview.com/1504-White-Papers-Application-Notes/147135-Pros-and-Cons-of-Using-Correlation-Versus-Multivariate-Algorithms-for-Material-Identification-via-Handheld-Spectroscopy/

De Castro, N., & Li, S. (2023, March). CHARACTERIZING SPECTRAL FEATURES OF WATER ICE, LUNAR REGOLITH ANALOGUES, AND THEIR MIXTURES AT THE VNIR REGION. *LPSC 2023*. Lunar and Planetary Science Conference, The Woodlands, Texas.

Edison, K., Andersen, C., Harford, K., Tokunaga, J., & Romo, R. (2021). The Effects of Mineral Abundances on Mechanical and Structural Properties of Sintered Hawaiian Basalt Aggregate: Implications for Lunar/Mars ISRU Applications. *Earth and Space 2021*, 818–831. https://doi.org/10.1061/9780784483374.076

FieldSpec 4 User Manual. (2016). ASD Inc.

Flynn, L., Zhu, F., Li, S., & Andersen, C. (2021). *Autonomous Rover Operations for Planetary Surface Exploration using Machine Learning Algorithms* (2021 Established Program to Stimulate Competitive Research (EPSCoR)) [Grant Proposal]. NASA Office of STEM Engagement.

Gawronska, A. J., Barrett, N., Boazman, S. J., Gilmour, C. M., Halim, S. H., Harish, McCanaan, K., Satyakumar, A. V., Shah, J., Meyer, H. M., & Kring, D. A. (2020). Geologic context and potential EVA targets at the lunar south pole. *Advances in Space Research*, *66*(6), 1247–1264. https://doi.org/10.1016/j.asr.2020.05.035

Gwizd, S., Stack, K. M., Calef, F., Francis, R., Graff, J., Langley, C., Kristinsson, Þ. H., Thorarensen, V. P., Bernharðsson, E., Phillips, M., Moersch, J., Basu, U., & Voigt, J. R. C. (2023). *ROVER–AERIAL VEHICLE EXPLORATION NETWORK (RAVEN): MISSION PLANNING, IMPLEMENTATION, AND RESULTS FROM THE 2022 ROVER-ONLY FIELD CAMPAIGN AT*. *2806*.

Henschel, H., Andersson, A. T., Jespers, W., Mehdi Ghahremanpour, M., & van der Spoel, D. (2020). Theoretical Infrared Spectra: Quantitative Similarity Measures and Force Fields. *Journal of Chemical Theory and Computation*, *16*(5), 3307–3315. https://doi.org/10.1021/acs.jctc.0c00126

Henschel, H., & van der Spoel, D. (2020). An Intuitively Understandable Quality Measure for Theoretical Vibrational Spectra. *The Journal of Physical Chemistry Letters*, *11*(14), 5471–5475. https://doi.org/10.1021/acs.jpclett.0c01655

Imai, F. H., Rosen, M. R., & Berns, R. S. (2002). Comparative Study of Metrics for Spectral Match Quality. *Conference on Colour in Graphics, Imaging, and Vision*, *1*(1), 492–496. https://doi.org/10.2352/CGIV.2002.1.1.art00103

Kokaly, R. F., Clark, R. N., Swayze, G. A., Livo, K. E., Hoefen, T. M., Pearson, N. C., Wise, R. A., Lowers, H. A., Driscoll, R. L., & Klein, A. J. (2017). *USGS Spectral Library Version 7* (Data Series 1035, p. 61) [USGS Numbered Series]. U.S. Geological Survey.

Li, S., Lucey, P. G., Milliken, R. E., Hayne, P. O., Fisher, E., Williams, J.-P., Hurley, D. M., & Elphic, R. C. (2018). Direct evidence of surface exposed water ice in the lunar polar regions. *Proceedings of the National Academy of Sciences*, *115*(36), 8907–8912. https://doi.org/10.1073/pnas.1802345115

Milliken, R. (2020). *REFLECTANCE EXPERIMENT LABORATORY (RELAB) DESCRIPTION AND USER'S MANUAL* [Reflectance spectra and ancillary data]. https://doi.org/10.17189/1519032

Robinson, I., & MacArthur, A. (2011). *The Field Spectroscopy Facility Post Processing Toolbox User Guide: Post processing spectral data in MATLAB*. Natural Environment Research Council. http://www.mathworks.com/matlabcentral/fileexchange/31547-field-spectroscopy-facility-post-processing-toolbox

Romo, R., Andersen, C., Edison, K., & Musilova, M. (2021). Analog Field Sites on Hawai'i Island. *Earth and Space 2021*, 577–589. https://doi.org/10.1061/9780784483374.054

Sanders, G. B., Larson, W. E., Picard, M., & Hamilton, J. C. (2011). *Use of Hawaii Analog Sites for Lunar Science and In-Situ Resource Utilization*.

Spudis, D., Plescia, J., Bussey, B., Josset, J.-L., Beauvivre, S., & the Amie team. (2008, March). THE GEOLOGY OF THE SOUTH POLE OF THE MOON AND AGE OF SHACKLETON CRATER. *LPSC 2008*. Lunar and Planetary Science Conference, League City, Texas.

Ten Kate, I. L., Armstrong, R., Bernhardt, B., Blumers, M., Craft, J., Boucher, D., Caillibot, E., Captain, J., Deleuterio, G., Farmer, J. D., Glavin, D. P., Graff, T., Hamilton, J. C., Klingelhöfer, G., Morris, R. V., Nuñez, J. I., Quinn, J. W., Sanders, G. B., Sellar, R. G., … Zacny, K. (2013). Mauna Kea, Hawaii, as an Analog Site for Future Planetary Resource Exploration: Results from the 2010 ILSO-ISRU Field-Testing Campaign. *Journal of Aerospace Engineering*, *26*(1), 183–196. https://doi.org/10.1061/(ASCE)AS.1943-5525.0000200

The 2022 Eruption of Mauna Loa. (2023). Mauna Loa Solar Observatory (MLSO). https://www2.hao.ucar.edu/mlso/2022-eruption-of-mauna-loa

ViewSpec Pro User Manual. (2008). ASD Inc.

Wilhelms, D. E., Howard, K. A., & Wilshire, H. G. (1979). *Geologic map of the south side of the Moon* [USGS Numbered Series]. U.S. Geological Survey. https://doi.org/10.3133/i1162

Yingst, R. A., Russell, P., Ten Kate, I. L., Noble, S., Graff, T., Graham, L. D., & Eppler, D. (2015). Designing remote operations strategies to optimize science mission goals: Lessons learned from the Moon Mars Analog Mission Activities Mauna Kea 2012 field test. *Acta Astronautica*, *113*, 120–131. https://doi.org/10.1016/j.actaastro.2015.02.029